Heliyon 10 (2024) e37062

Contents lists available at ScienceDirect

Heliyon

journal homepage: www.cell.com/heliyon

Research article

circ_0114866 promotes the progression and EMT of non-small cell lung cancer via miR-653-5p/MYL6B axis

Jinpeng Sun [a,*], Zhenshan Zhang [b], Binghui Xia [a], Tianyu Yao [c], Fengyue Ge [d], Fengmei Yan [e]

[a] Department of General Surgery Ward,Cangzhou Hospital of Integrated TCM-WM·Hebei China
[b] Department of Medical Oncology, Cangzhou Hospital of Integrated TCM-WM·Hebei, China
[c] Department of Cardiology, Cangzhou Hospital of Integrated TCM-WM·Hebei, China
[d] Department of Functional Examination, Cangzhou Hospital of Integrated TCM-WM·Hebei, China
[e] Department of Endoscopic Diagnosis and Treatment Center, Cangzhou Hospital of Integrated TCM-WM·Hebei, China

A B S T R A C T

Background: Non-small-cell lung cancer (NSCLC) is the most prevalent form of lung cancer. Circular RNA (circRNA) has emerged as a key player in the development of NSCLC by acting as miRNA sponges. However, the precise role of circ_0114866 in regulating NSCLC process is yet to be elucidated.

Methods: The expression of circ_0114866, miR-653-5p, and MYL6B were assessed by qPCR. Cell viability, proliferation, invasion, and migration were investigated using CCK-8, colony formation, Transwell, and wound healing assays. The protein levels of MYL6B, MMP-2, N-cadherin, E-cadherin, and vimentin were evaluated through Western blot analysis. Xenograft tumor model were selected to analyze the impact of circ_0114866 on NSCLC tumor growth. Through circBank or Starbase databases, the binding interactions between miR-653-5p and circ_0114866 or MYL6B were predicted. Subsequently, these interactions were verified by dual-luciferase reporter assay.

Results: The expression of circ_0114866 and MYL6B were clearly elevated, while miR-653-5p expression was notably reduced in NSCLC tissues and cells. Notably, circ_0114866 knockdown obviously suppressed the proliferation, metastasis, and EMT process in NSCLC cells. Additionally, circ_0114866 functioned as a sponge for miR-653-5p, leading to an increase in MYL6B expression by absorbing miR-653-5p. Furthermore, the inhibitory effects on biological behaviors and EMT process of NSCLC cells induced by circ_0114866 knockdown were reversed by miR-653-5p inhibitor. Moreover, *in vivo* experiments demonstrated that silencing circ_0114866 resulted in a repression of tumor growth.

Conclusion: Our findings indicate that circ_0114866 knockdown upregulated MYL6B transcription by sponging miR-653-5p, leading to hinder the progression and EMT process of NSCLC.

1. Introduction

Lung cancer serves as the most prevalent common cancer, approximately 2 million new cases are diagnosed annually worldwide [1,2]. Non-Small Cell Lung Cancer (NSCLC) accounts for more than 80 % of all lung cancer cases [3]. Unfortunately, a significant number of NSCLC patients receive a late-stage diagnosis due to factors such as limited adoption of screening protocols and the absence of discernible clinical symptoms in the early stages of the disease [4]. This delayed diagnosis leads to a grim prognosis for NSCLC patients, despite considerable progress in surgical interventions, immunotherapy, and pharmacological treatments over the past two decades [5]. Currently, the five-year survival rate for lung cancer patients is only around 20 % [6]. Consequently, there is an urgent need to discover new biomarkers for NSCLC.

* Corresponding author.
E-mail address: wohenwocao@126.com (J. Sun).

https://doi.org/10.1016/j.heliyon.2024.e37062
Received 20 October 2023; Received in revised form 21 August 2024; Accepted 27 August 2024

Circular RNA (circRNA) is a distinctive type of non-coding RNA. Unlike linear RNA, circRNA possesses covalent closed-loop structure, and this unique structure contributes to enhance the stability of circRNA [7]. Initially, circRNA was perceived as a byproduct resulting from mRNA mis-splicing, and it was believed to lack any significant biological function [8]. However, recent studies have unveiled that circRNA molecules were abundant in miRNA binding sites, serving as miRNA sponges in cells [9], contribute to the onset and progression of diverse cancer types, and hold promise as novel targets for cancer diagnosis and therapy [10,11]. Numerous studies highlight the critical regulatory role of circRNA in the progression of various cancers, including NSCLC [12]. For instance, circ_0074027 has been identified as a miR-433-3p sponge, thereby promoting the proliferation and metastasis of NSCLC cells through upregulating IGF1 expression [13]. Additionally, Han et al. observed that the upregulation of circ-RAD23B expression contributes to the malignant progression of NSCLC [14]. Nevertheless, the majority of circRNAs' function in NSCLC remains undefined.

Numerous studies have highlighted that miRNA participated in various cellular processes by mediating degradation or inhibit translation of their target mRNA [15,16]. In the context of human cancers, miRNA exhibited dual functionality, serving as either oncogenes or tumor suppressors throughout tumor development and progression [17]. Notably, miR-653-5p has emerged as a potent tumor repressor. Studies have demonstrated that miR-653-5p effectively impeded cervical cancer progression by targeting MAPK6 [18]. Moreover, miR-653-5p exerted its inhibitory effects on ovarian cancer cell proliferation and metastasis by modulating ELF2 expression [19]. Furthermore, miR-653-5p acted as a sponge for circARL8B, restraining breast cancer advancement and fatty acid metabolism through suppressing HMGA2 expression [20]. However, whether circ_0114866 can participate in NSCLC progression by sponging miR-653-5p was still ambiguous.

Myosin is a superfamily of motor proteins [21]. These motor proteins utilize the energy generated by ATP hydrolysis to engage with actin filaments, functioning as essential molecular motors [22]. The majority of Myosin was composed of heavy and light chains, including the myosin heavy chain, regulatory light chain, and essential light chain [23]. Among these components, MYL6B was a pivotal light chain in non-muscle myosin II, which is involved in several biological processes, including cell adhesion, cell migration, endocytosis, and cargo transport [24,25]. Research has suggested that MYL6B was dysregulated in tumor tissues and had a close association with EMT [26]. Furthermore, we found that MYL6B contains binding sites for miR-653-5p through circBank database.

In our investigation, we detected circ_0114866 expression was significantly elevated in NSCLC. Through a series of experiments, we demonstrated that circ_0114866 plays a pivotal role in promoting NSCLC cell proliferation, invasion, metastasis, and EMT process via miR-433-3p/MYL6B axis.

2. Materials and methods

2.1. Human tissue samples

This study included 30 patients pathologically diagnosed with NSCLC at Cangzhou Central Hospital. The inclusion criteria were: patients pathologically diagnosed with NSCLC, absence of distant metastasis, normal function of major organs, and age between 18 and 80 years. The exclusion criteria were: presence of other lung diseases, other malignant tumors, history of drug abuse, metabolic or endocrine diseases, any infection or chronic active inflammation, or refusal to consent to sampling. In this study, we collected tumor

Table 1
Demographic characteristics of NSCLC patients.

Variable	Number of Patients
All patients	30
Gender	
Male	18
Female	12
Age	
≤60	9
> 60	21
Histopathological type	
AC	17
SCC	13
pTMN	
pT1	7
pT2	18
pT3	5
Size of tumor	
≤1 cm	2
1–2 cm	2
2–3 cm	3
3–4 cm	11
4–5 cm	7
> 5 cm	5
Pack-years (PYs)of smoking	
≤30 PYs	11
31–45 PYs	13
> 45 PYs	7

tissues and corresponding adjacent non-cancerous tissues from the patients diagnosed with NSCLC to detect the expression of related genes. Prior to their inclusion, explicit informed consent was obtained from all participating patients. Demographic features of NSCLC patients were described in Table 1.

2.2. Main reagent

RPMI-1640 medium (Gibco, USA), Fetal Bovine Serum (FBS, Hyclone, USA), Lipofectamine 2000 (Invitrogen, USA), puromycin (Santa Cruz Biotechnology, USA), CCK8 kit (Beyotime Biotechnology, China), diluted Matrigel (BD Biosciences, USA), THSG (Sigma, USA), RNase R (Lucigen, USA), RNeasy MinElute Cleanup kit (Qiagen, China), TRIzol Reagent (Invitrogen, USA), MicroRNA Reverse Transcription kit (Thermo USA), First-Strand cDNA kit and SYBR Green kit (Tiangen, China), RIPA and PMSF were the products of Beyotime (Beyotime Biotechnology, China), BCA kit (Solaibao, China).

2.3. Cell culture

Human lung cancer cell lines (H1299, PC9, H358 and A549) and normal human lung control cell line (BEAS-2B) were cultured in RPMI-1640 medium (plus 10 % FBS). To maintain sterility, we added 80 U/ml Penicillin-Streptomycin. These five cell lines were cultured at 37 °C and 5 % CO2.

2.4. Cell transfection

In present study, si-circ_0114866, miR-653-5p inhibitor, miR-653-5p mimic, MYL6B overexpression plasmid, and their negative controls were utilized for cell transfection. Target sequences are listed in Table 2. As a control, an empty vector plasmid was utilized. Transient transfection of H358 and A549 cells was conducted using Lipofectamine 2000. After a 72-h transfection period, we selected stably transfected H358 and A549 cells by subjecting them to treatment with 2 μg/ml puromycin.

2.5. Quantitative PCR (qPCR)

Total RNA was extracted from H358 and A549 cells and tumor tissues using TRIzol Reagent. Following this, cDNA was synthesized using either the MicroRNA Reverse Transcription kit or the First-Strand cDNA kit. Subsequently, qPCR was carried out using the SYBR Green kit. The qPCR reaction was set 40 cycles of 94 °C for 5 min and 94 °C for 20 s; 60 °C for 1 min; Collect signals at 60 °C. In order to perform relative quantitative analysis, internal references such as GAPDH and U6 were utilized. The $2^{-\triangle\triangle CT}$ method was employed for data analysis in this study. Primer sequences are shown in Table 3.

2.6. RNase R assay

The stability of circ_0114866 was evaluated using the RNase R assay following the manufacturer's instructions. Briefly, total RNA was extracted from H358 and A549 cells. Subsequently, 2 mg of total RNA was subjected to a 30-min incubation at 37 °C with or without RNase R (3U/mgR). Purification was then performed using the RNeasy MinElute Cleanup kit, and circ_0114866 expression was assessed by qRCR.

2.7. Cell viability assay

Cell viability was assessed utilizing the CCK8 assay. Briefly, 1 × 103 H358 and A549 cells were cultivated in a 96-well plate. Culture medium was substituted with a gradient of THSG concentrations following 24 h incubation. After additional 12, 24, and 48 h of culture, the supernatant was aspirated, and CCK8 (20 μL) was introduced into each well. Using a microplate reader, the OD value at 490 nm was detected.

2.8. Colone formation assay

H358 and A549 cells were initially seeded onto 6-well plates and treated with JB at different concentrations for 24 h. After this treatment, H358 and A549 cells were harvested, counted, and reseeded into new 6-well plates (500 cells per well). Following a 2-week incubation period, H358 and A549 cells were fixed with pure methanol and stained with a 0.5 % crystal violet solution. Finally, the

Table 2
Target sequences.

ID	Sequences (5′-3′)
si-circ_0114866	AGUCCACCCUAGAGAAUGGCA
miR-653-5p mimic	GUGUUGAAACAAUCUCUACUG
miR-653-5p inhibitor	CAGUAGAGAUUGUUUCAACAC
MYL6B	CAUCCCAGACUCCCUGGCUAUUUA

Table 3
Primer sequence.

Gene	Forward (5'→3')	Reverse (5'→3')
hsa_circ_0114866	GTTGAGCCTGTCGTCTCCTA	TTCATCCTTGAGGCCGTTCA
ZNF337	TTCAAACCCGGGGAGACAG	GGGATCTGGCCAAAAGGTCT
miR-653-5p	GCGCGGTGTTGAAACAATCT	AGTGCAGGGTCCGAGGTATT
MYL6B	CATCCCAGACTCCCTGGCTATTTA	CTCCTGGGTTTTCTGAGGGG
U6	GCTTCGGCAGCACATATACTAA	AACGCTTCACGAATTTGCGT
GAPDH	GACCACAGTCCATGCCATCAC	ACGCCTGCTTCACCACCTT

colonies were photographed and quantified.

2.9. Cell invasion assay

The inserts were coated with 20 μL of 1:2-diluted Matrigel, and then treated with varying concentrations of THSG for 24 h. Subsequently, 1 × 105 H358 and A549 cells were transferred to the upper chamber of the Matrigel-coated inserts, which contained 100 μL serum-free medium. Following 24 h incubation, the lower chamber was stuffed with a substance supplemented with 10 % FBS. After incubation, 0.1 % crystal violet was used to stain filters, and cell morphology was observed using an Olympus microscope (Japan).

2.10. Wound healing assay

In six-well plates, H358 and A549 cells were planted and grew to 90 % confluence. Following this, serum-free DMEM replaced the culture medium. Once the cell monolayers had achieved confluence, a scratch was generated using 100 μL sterile pipette tips. After creating the scratch, the wells were washed twice with fresh medium to remove any cells from the scratched area, and the old medium was replaced with medium containing 1 % FBS. Subsequently, the cells were exposed to varying concentrations of MCL. Following 48 h of MCL incubation, the wound was examined using a Leica DM 14000B optical microscope (Germany).

2.11. Dual-luciferase reporter (DLR) assay

WT-circ_0114866, MUT-circ_0114866, WT-MYL6B and MUT-MYL6B were created by integrating the binding sites of wild-type (WT) and mutant (MUT) miR-653-5p with VEGF fragments within the pmirGLO vector. Lipofectamine 2000 (Qiagen, USA) was employed for the transfection of these vectors into H358 and A549 cells. After 48 h, H358 and A549 cells were collected using a passive lysis buffer, followed by the measurement of luciferase activity using the GloMax® 20/20 luminometer (Promega, USA).

2.12. Western blot

The protein was extracted by RIPA combined with PMSF. After measuring the protein concentration using the BCA kit, proteins were transferred to the PVDF membrane. Seal the membrane with skim milk, dilute the first antibody to a certain volume and incubate it overnight at 4 °C. After washing, incubate the corresponding second antibody for 2 h, and expose the target band in a chemiluminescent solution. Prime Western Blotting Reagent (Cytiva, UK) detected protein bands, and Image J analyzed band grey values.

2.13. In vivo studies

A total of 10 male nude mice were included in this study. Animal experiments adhered to institutional guidelines to ensure ethical conduct. NSCLC cells were genetically modified through stable transfection using various constructs, including sh-NC and sh-circ_0114866. Subsequently, nude mice had 1 × 106 cells injected into their right flanks, and the tumors volumes were measured with vernier caliper at 5-d intervals. After a 22-d period post-tumor implantation, the mice were euthanized, and the tumor weight was determined.

2.14. Immunohistochemistry

The paraffin sections were deparaffinized for antigen retrieval. Subsequently, sections were incubated with primary antibody Ki67, and incubated overnight at 4 °C. The following day, sections were washed with PBS. A diluted secondary antibody was then applied and incubated at room temperature for 50 min. After washing with PBS, DAB color developing solution was carefully applied dropwise. Following the color reaction, counterstaining with hematoxylin was performed to shift the hue back to blue. The sections were then dehydrated, made transparent, and dried before observation under a microscope.

2.15. Statistical analysis

GraphPad Prism 7.0 software was used to analyze the data. Continuous data was represented using the format mean ± standard deviation (x ± s). To compare between two groups, we employed the *t*-test. For comparing multiple groups, we utilized the one-way ANOVA. Finally, for pairwise comparisons, we employed the LSD-T test. We consider P less than 0.05 represented a statistically significant difference.

3. Results

3.1. circ_0114866 expression in NSCLC tissues and cell lines

Compared to adjacent normal lung tissues, circ_0114866 expression was significantly elevated in NSCLC tissues (Fig. 1A). Furthermore, circ_0114866 expression also exhibited a substantial increase in all NSCLC cell lines when compared to BEAS-2B cells (Fig. 1B). H358 and A549 cells were selected for subsequent experiments due to their highest circ-0114866 expression. Circ_0114866 is derived from the ZNF337 gene. RNase R assay results showed that circ_0114866 was resistant to RNase R treatment, while ZNF337 mRNA was sensitive to RNase R digestion (Fig. 1C and D). Additionally, in H358 and A549 cells, circ_0114866 was found to be expressed in the cytoplasm and the nucleus, with a significantly higher expression level observed in the cytoplasm (Fig. 1E and F).

3.2. Influences of circ_0114866 on the proliferation, migration, invasion and EMT process of NSCLC cells

Next, H358 and A549 cells were transfected with si-NC or si-circ_0114866. qPCR results found a significant reduction in circ_0114866 expression upon si-circ_0114866 transfection (Fig. 2A). Moreover, CCK-8 assay demonstrated that si-circ_0114866 led to a notable reduction in H358 and A549 cell viability (Fig. 2B). Moreover, clone formation assay revealed that si-circ_0114866 effectively reduced H358 and A549 cell proliferation (Fig. 2C). Furthermore, cell migration and invasion were evaluated through Transwell and wound healing assays, demonstrating that si-circ_0114866 effectively suppressed H358 and A549 cell metastasis (Fig. 2D and E). Western blot analyses indicated that si-circ_0114866 reduced expression of MMP-2, N-cadherin, and vimentin, while increased E-cadherin expression in H358 and A549 cells (Fig. 2F and G).

3.3. Influences of circ_0114866 on NSCLC tumor growth in vivo

To investigate circ_0114866's impact on NSCLC tumor growth *in vivo*, we established stable A549 cell lines transfected with either sh-circ_0114866 or sh-NC. qPCR results demonstrated a significant reduction in circ_0114866 expression in A549 cells transfected with

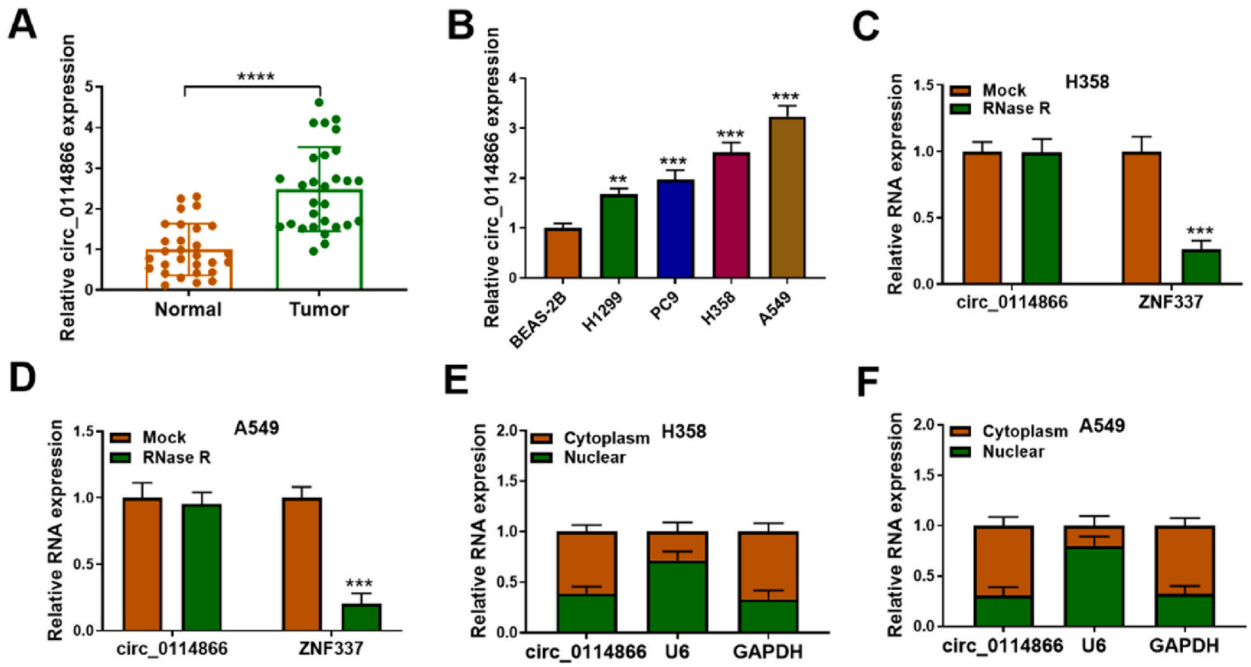

Fig. 1. The expression of circ_0114866 in NSCLC tissues and cell lines. (A) Circ_0114866 expression in NSCLC tissues. (B) Circ_0114866 expression in BSAE-2B, H1299, PC9, H358 and A549 cells. (C–D) The stability of circ_0114866 in H358 and A549 cells. (E–F) The subcellular localization for circ_0114866 in H358 and A549 cells. $^{**}P < 0.01$; $^{***}P < 0.001$.

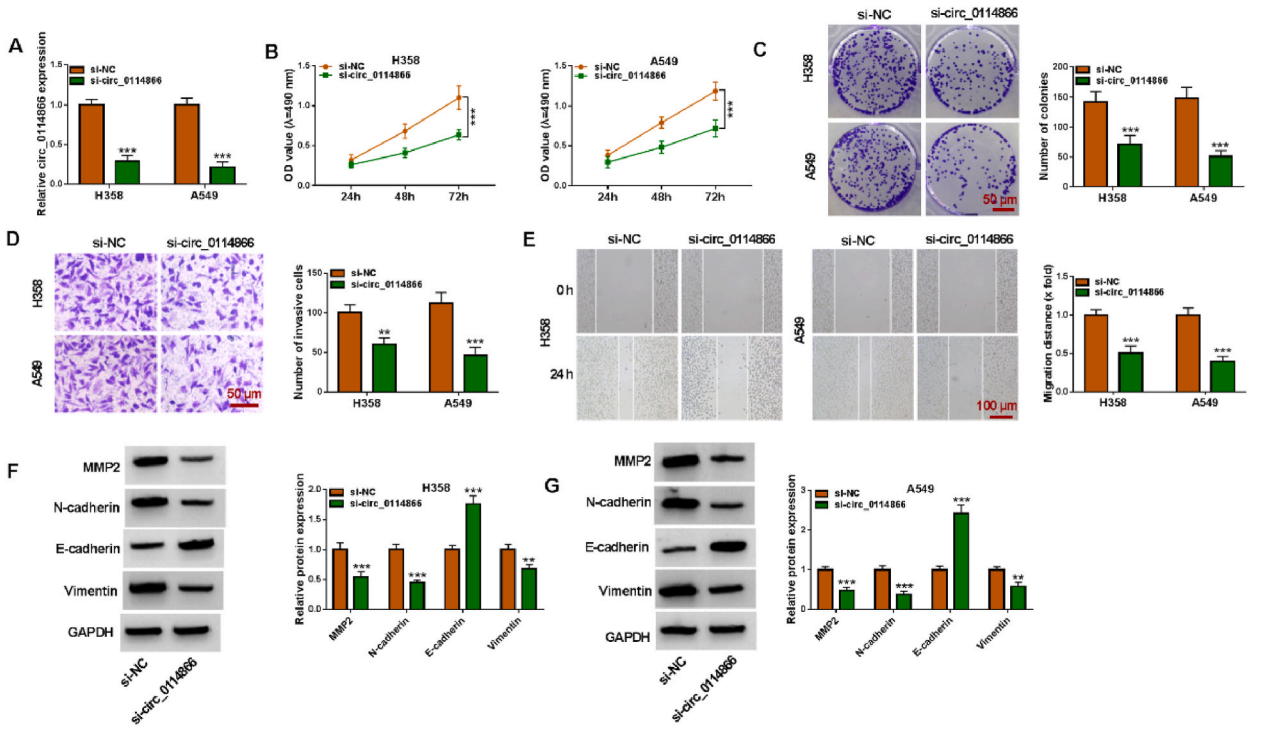

Fig. 2. Inhibition of circ_0114866 suppressed the proliferation, migration, invasion and EMT process of NSCLC cells. (A) Circ_0114866 expression in H358 and A549 cells. (B) Cell viability in H358 and A549 cells in each group. (C) Cell proliferation in H358 and A549 cells in each group. (D) Cell migration in H358 and A549 cells in each group. (E) Cell invasion in H358 and A549 cells in each group. (F–G) The protein levels of MMP-2, N-cadherin, E-cadherin and vimentin in H358 and A549 cells. $^{**}P < 0.01$; $^{***}P < 0.001$. Full Western blot images can be found at Supplementary Materials.

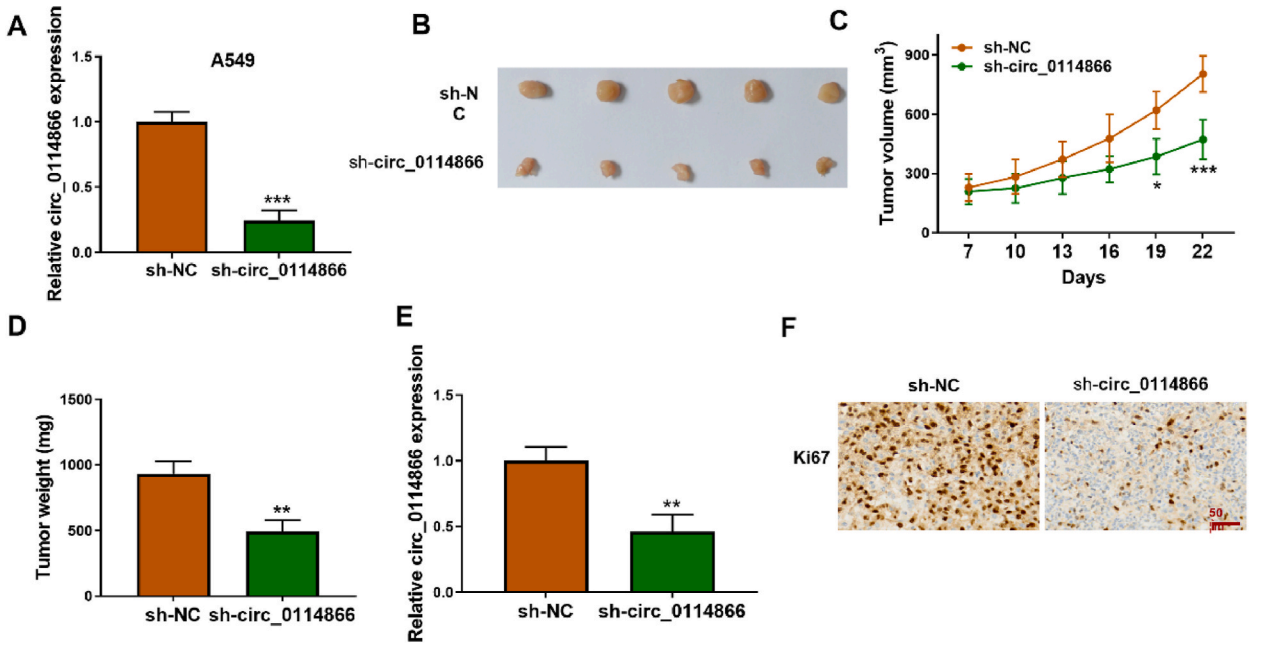

Fig. 3. Inhibition of circ_0114866 inhibited NSCLC tumor growth *in vivo*. (A) Circ_0114866 expression in A549 cells. (B) Representative pictures of tumor tissues in each group. (C) Tumor volumes at different days after injection in each group. (D) Tumor weights in each group. (E) Circ_0114866 expression in tumor tissues. $^{**}P < 0.01$; $^{***}P < 0.001$.

sh-circ_0114866 (Fig. 3A). In the sh-circ_0114866 group, we observed a substantial reduction in tumor volume and weight when compared to the sh-NC group (Fig. 3B–D). Moreover, tumor tissues from the sh-circ-MBOAT2 group exhibited a noteworthy decrease in circ_0114866 expression compared to those from the sh-NC group (Fig. 3E). Additionally, immunohistochemical staining demonstrated that sh-circ_0114866 significantly decreased Ki67 expression in NSCLC tumor tissues (Fig. 3F).

3.4. Circ_0114866 acted as a miR-653-5p sponge

To investigate the potential mechanism of circ_0114866 in NSCLC progression, we identified candidate miRNA targets for circ_0114866 using circBank database. Our analysis pinpointed miR-653-5p had a potential binding site with circ_0114866 (Fig. 4A). To substantiate that circ_0114866 serves as a sponge for miR-653-5p, we transfected miR-653-5p mimic or miR-NC into H358 and A549 cells. qPCR results found miR-653-5p mimic significantly increased miR-653-5p expression in H358 and A549 cells (Fig. 4B). DLR results demonstrated a significant reduction in the relative luciferase activity of the WT-circ_0114866 3' UTR in the miR-653-5p mimic group, whereas the relative luciferase activity of MUT-circ_0114866 3' UTR was no discernible difference between two groups (Fig. 4C and D). Moreover, transfection with miR-653-5p mimic led to a noticeable decrease in circ_0114866 expression in H358 and A549 cells (Fig. 4E). Furthermore, we observed a significant reduction in miR-653-5p expression in tumor tissues (Fig. 4F). Correlation analysis also revealed a negative association between circ_0114866 expression and miR-653-5p expression within tumor tissues (Fig. 4G). Additionally, miR-653-5p expression exhibited a significant decrease in H358 and A549 cells when compared to BEAS-2B cells (Fig. 4H).

3.5. Circ_0114866 knockdown inhibited the proliferation, migration, invasion and EMT process of NSCLC cells by sponging miR-653-5p

We next reduced the expression of miR-653-5p by transfecting miR-653-5p inhibitor. qPCR results revealed a significant reduction in miR-653-5p expression upon transfection with miR-653-5p inhibitor (Fig. 5A). Subsequently, we observed that transfecting si-circ_0114866 alone led to a substantial increase in miR-653-5p expression, while co-transfection of si-circ_0114866 and the miR-653-5p inhibitor reversed this trend (Fig. 5B). In H358 and A549 cells, miR-653-5p inhibitor mitigated the suppressive effects of si-circ_0114866 on cell viability and proliferation (Fig. 5C and D). Furthermore, miR-653-5p inhibitor counteracted the inhibitory effects of si-circ_0114866 on metastasis of H358 and A549 cells (Fig. 5E-H). Besides, miR-653-5p inhibitor also reversed the inhibitory effects of si-circ_0114866 on the EMT process (Fig. 5I and J).

3.6. miR-653-5p directly targeted MYL6B

Utilizing Starbase database, we identified a binding site between miR-653-5p and MYL6B (Fig. 6A). Furthermore, DLP results demonstrated a significant decrease in relative luciferase activity of WT-MYL6B 3' UTR in the miR-653-5p mimic group, while the relative luciferase activity of MUT-MYL6B 3' UTR was no noticeable difference between two groups (Fig. 6B and C). Subsequently, Western blot analyses revealed a substantial reduction in MYL6B expression upon transfection with the miR-653-5p mimic in H358 and A549 cells (Fig. 6D). Moreover, MYL6B mRNA and protein levels were notably increased in tumor tissues (Fig. 6E & G). Correlation analysis unveiled a negative association between miR-653-5p expression and MYL6B expression within tumor tissues (Fig. 6F). Additionally, MYL6B expression was significantly elevated in H358 and A549 cells when compared to BEAS-2B cells (Fig. 6H).

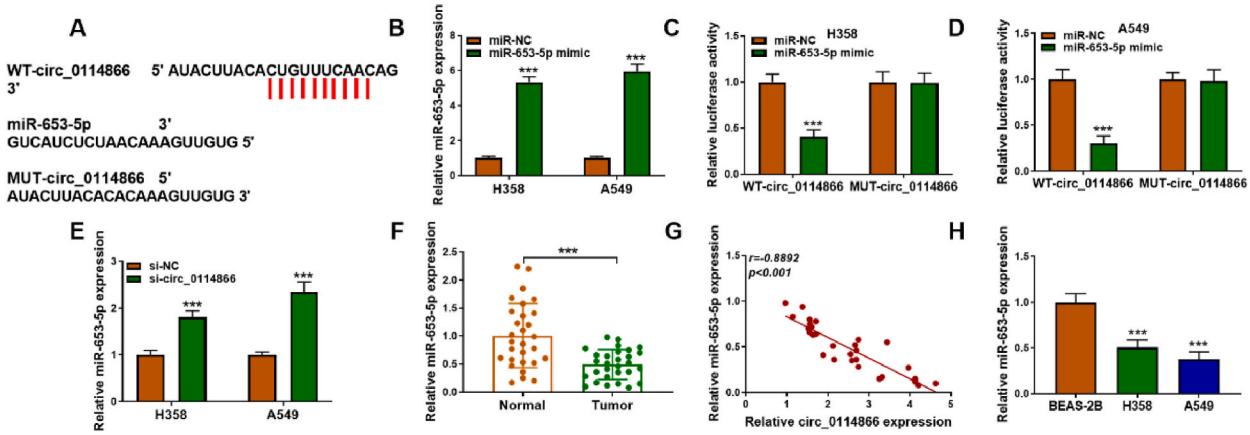

Fig. 4. Circ_0114866 acted as the sponge of miR-653-5p. (A) The binding sites between circ_0114866 and miR-653-5p. (B) MiR-653-5p expression in H358 and A549 cells. (C–D) Fluorescence intensity of circ_0114866 3′UTR in H358 and A549 cells in each group. (E) MiR-653-5p expression in H358 and A549 cells. (F) MiR-653-5p expression in NSCLC tissues. (G) The correlation between circ_0114866 expression and miR-653-5p expression in NSCLC tissues. (H) MiR-653-5p expression in BSAE-2B, H358 and A549 cells. ***$P < 0.001$.

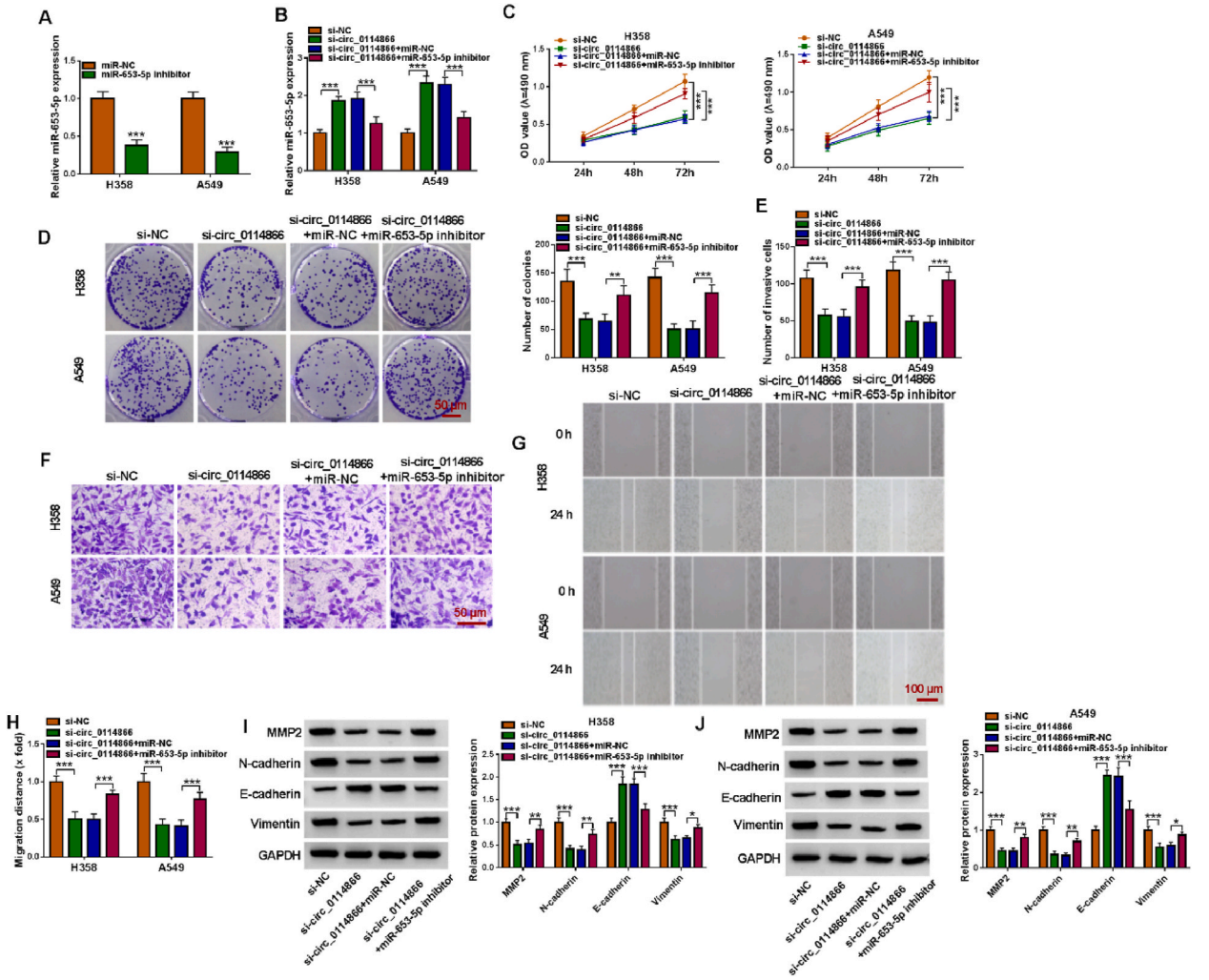

Fig. 5. Circ_0114866 knockdown suppressed the proliferation, migration, invasion and EMT process of NSCLC cells by absorbing miR-653-5p. (A) MiR-653-5p expression in H358 and A549 cells. (B) MiR-653-5p expression in H358 and A549 cells in each group. (C) Cell proliferation in H358 and A549 cells in each group. (D) Cell proliferation in H358 and A549 cells in each group. (E–F) Cell invasion in H358 and A549 cells in each group. (G–H) Cell migration in H358 and A549 cells in each group. (I–J) The protein levels of MMP-2, N-cadherin, E-cadherin and vimentin in H358 and A549 cells. $*P < 0.0$; $**P < 0.01$; $***P < 0.001$. Full Western blot images can be found at Supplementary Materials.

3.7. miR-653-5p suppressed the proliferation, migration, invasion and EMT process of NSCLC cells by targeting MYL6B

To investigate the potential regulatory role of miR-653-5p on NSCLC progression through its interaction with MYL6B, we transfected pcDNA/MYL6B into H358 and A549 cells to increase MYL6B expression. Notably, we observed a significant elevation in MYL6B expression in the MYL6B group when compared to the pcDNA group (Fig. 7A). Subsequently, we found MYL6B overexpression had a mitigating effect on the downregulation of MYL6B induced by miR-653-5p mimic (Fig. 7B). CCK-8 and cell colony formation assays revealed that the introduction of the miR-653-5p mimic resulted in a notable reduction in the viability and proliferation of H358 and A549 cells, while the overexpression of MYL6B attenuated these effects (Fig. 7C and D). Moreover, miR-653-5p mimic inhibited the metastasis of H358 and A549 cells. However, this inhibitory effect was counteracted by MYL6B overexpression (Fig. 7E-H). Furthermore, miR-653-5p mimic facilitated the EMT process, while MYL6B overexpression reversed this process (Fig. 7I and J).

3.8. Circ-0114866 knockdown reduced MYL6B expression by sponging miR-653-5p

In prior experiments, it was substantiated that circ_0114866 acted as a miR-653-5p sponge, and MYL68 served as a target gene of miR-653-5p. As a consequence, it is reasonable to postulate that circ-0114866 can regulate MYL6B expression by sponging miR-653-5p in H358 and A549 cells. Western blot analyses unveiled that the introduction of si-circ-0114866 elicited a significant reduction in mRNA and protein levels of MYL6B. Nevertheless, the transfection of miR-653-5p inhibitor effectively reversed this aforementioned

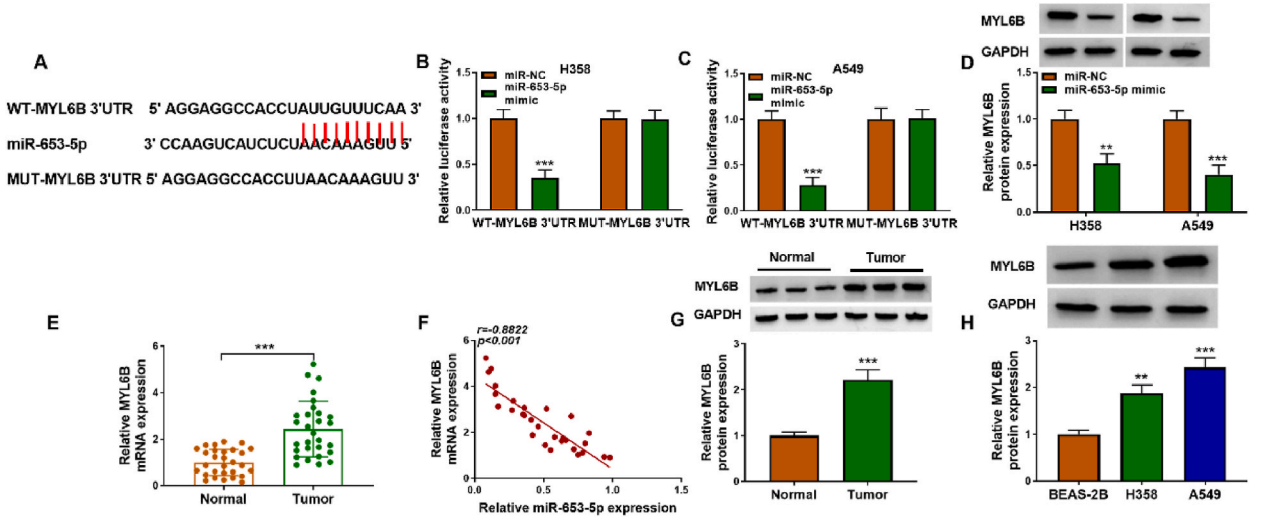

Fig. 6. MiR-653-5p was bound to MYL6B and suppressed its expression. (A) The binding sites between miR-653-5p and MYL6B. (B–C) Fluorescence intensity of MYL6B 3′UTR in H358 and A549 cells in each group. (D) The protein level of MYL6B in H358 and A549. (E) The mRNA level of MYL6B in NSCLC tissues. (F) The correlation between miR-653-5p expression and MYL6B expression in NSCLC tissues. (G) The protein level of MYL6B in NSCLC tissues. (H) e protein level of MYL6B in BSAE-2B, H358 and A549 cells. $^{**}P < 0.01$; $^{***}P < 0.001$. Full Western blot images can be found at Supplementary Materials.

effect (Fig. 8A-D).

4. Discussions

NSCLC, responsible for over 80 % of global lung cancer cases, is the primary cause of cancer-associated mortality [27]. Although substantial advancements have been achieved in the early detection and therapeutic approaches for NSCLC, the overall prognosis for patients remains discouraging [28]. CircRNA, characterized by covalent closed loop structure, was initially regarded as a byproduct of mRNA splicing without performing biological function [29]. However, emerging evidence underscores circRNAs' function in regulating NSCLC advancement by acting as miRNA sponges. One study revealed that circVMP1 regulated METTL3 and SOX2 expression by sponging miR-524-5p, thereby promoting NSCLC progression and cisplatin resistance [30]. Another investigation demonstrated circ_101237 strengthened NSCLC cells proliferation and metastasis via miR-490-3p/MAPK1 axis [31]. Hence, investigating the underlying mechanisms of circRNAs in NSCLC assumes paramount importance.

In previous investigation, we detected that circ_0114866 was significantly upregulated in NSCLC tissues through high-throughput sequencing and bioinformatics analysis (unpublished). In spite of this, the precise role of circ_0114866 in the progression of NSCLC has not been reported. In the current study, we confirmed circ_0114866 expression was remarkably elevated in NSCLC tissues and cell lines, suggesting its potential pivotal role in NSCLC. To elucidate the exact function of circ_0114866 in NSCLC, we employed si-circ_0114866 to downregulate its expression in NSCLC cell lines H358 and A549. The results unequivocally demonstrated that circ_0114866 silencing significantly attenuated the proliferation, migration, invasion, and EMT process of NSCLC cells. Furthermore, our findings also found that circ_0114866 knockdown had an obvious inhibitory effect on NSCLC tumor growth *in vivo*. Collectively, these findings strongly support the notion that circ_0114866 knockdown can effectively impede NSCLC progression.

Cytoplasmic and nuclear RNA analysis revealed that circ_0114866 mainly localized to the cytoplasm, suggesting circ_0114866 primary functioned at post-transcriptional level. A growing body of literature underscores the pivotal role of circRNA in modulating cancer progression by sponging miRNA [32]. Thus, we employed circBank database to identify potential candidate miRNAs, pinpointing miR-653-5p had a potential binding site with circ_0114866. Previous studies have reported miR-653-5p, acted as a cancer repressor, was downregulated in various cancer types, including cervical cancer [33], prostate cancer [34] and gastric cancer [35]. An experimental study indicated miR-653-5p suppressed the development of breast cancer [18]. Furthermore, circRANGAP1 enhanced the expression of COL11A1 by sponging miR-204-3p, thereby promoting NSCLC proliferation and metastasis [36]. In current study, we identified a significant reduction in miR-653-5p expression in NSCLC. Furthermore, we observed that miR-653-5p overexpression mitigated the malignant characteristics of NSCLC by restraining cell proliferation and metastasis. Additionally, we assessed the protein levels of EMT markers in NSCLC cells, revealing that miR-653-5p overexpression inhibited the EMT process. Our correlation analysis results indicated a negative association between circ_0114866 expression and miR-653-5p expression in NSCLC tissues. Moreover, we demonstrated that miR-653-5p inhibitor attenuated the inhibitory effects on NSCLC development and the EMT process induced by si-circ_0114866.

We next searched for the target gene of miR-653-5p using Starbase database. Ultimately, our investigation led us to identify MYL6B as a potential target gene, and the prediction was validated through DLP. Prior research has elucidated that MYL6B, as part of NMII

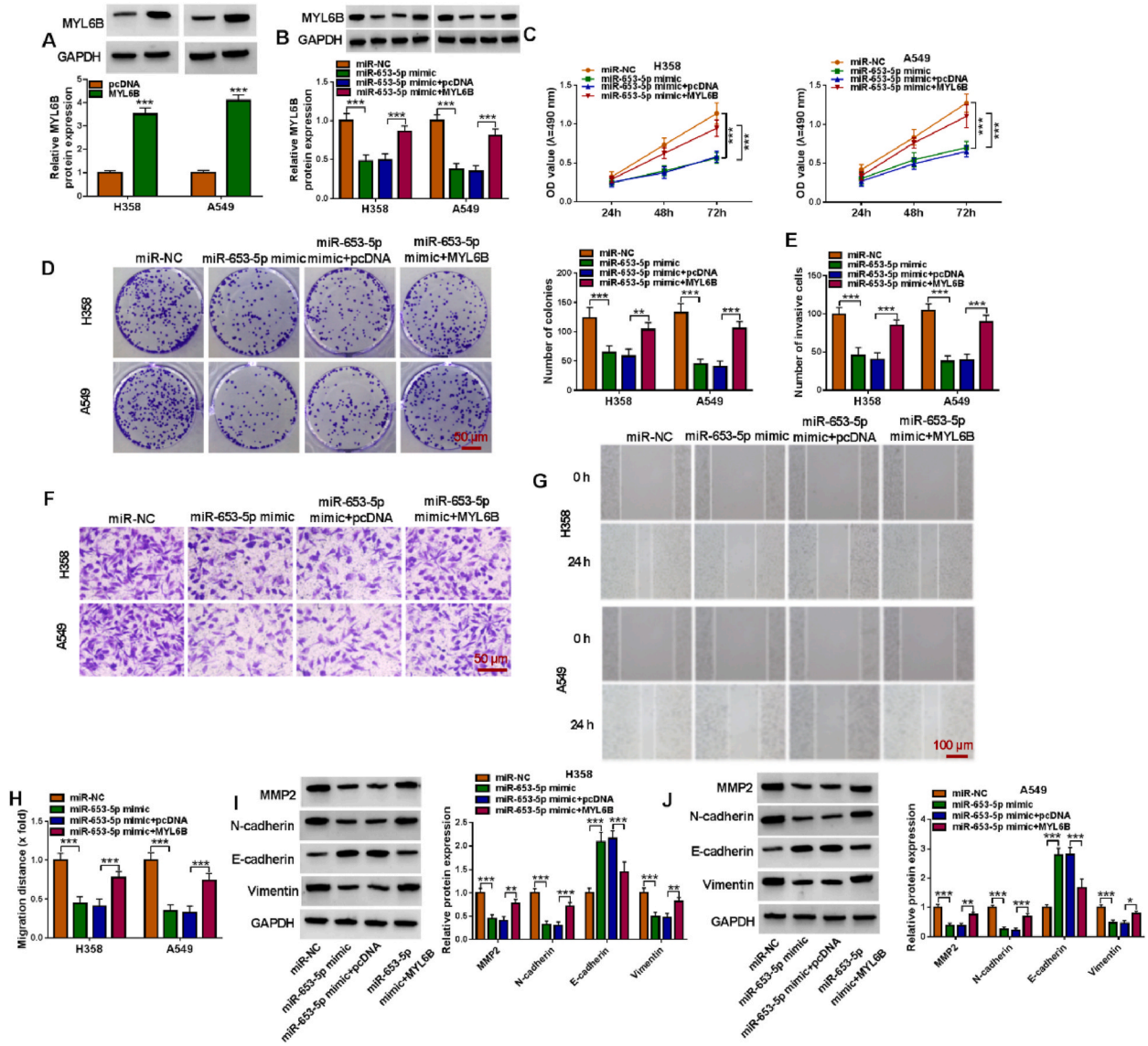

Fig. 7. miR-653-5p suppressed the proliferation, migration, invasion and EMT process of NSCLC cells by binding to MYL6B. (A) The protein level of MYL6B in H358 and A549 cells. (B) The protein level of MYL6B in H358 and A549 cells in each group. (C) Cell proliferation in H358 and A549 cells in each group. (D) Cell proliferation in H358 and A549 cells in each group. (E–F) Cell invasion in H358 and A549 cells in each group. (G–H) Cell migration in H358 and A549 cells in each group. (I–J) The protein levels of MMP-2, N-cadherin, E-cadherin and vimentin in H358 and A549 cells. $^{*}P < 0.0$; $^{**}P < 0.01$; $^{***}P < 0.001$. Full Western blot images can be found at Supplementary Materials.

holoenzymes, exerted its function in suppressing p53 activity [37]. Xie et al. identified that MYL6B was a driver gene in tumorigenesis and could expedite HCC progression by facilitating p53 degradation [26]. Our results revealed that MYL6B expression was notably enhanced in NSCLC. Through a series of molecular biology experiments, we have further demonstrated that MYL6B overexpression can effectively counteract the inhibitory effects of miR-653-5p on NSCLC progression and EMT process.

Lastly, Western blot analyses were conducted to corroborate the connection between circ_0114866 expression and MYL6B expression in NSCLC cells. Our findings demonstrated that circ_0114866 knockdown resulted in a notable reduction in MYL6B expression. Conversely, miR-653-5p inhibitor partially mitigated this effect, suggesting that circ_0114866 modulated MYL6B expression by sponging miR-653-5p.

Our study has some innovations. Our study found for the first time that circ_0114866 was upregulated in NSCLC. In addition, circ_0114866 regulates MYL6B expression by binding to miR-653-5p, thereby participating in the progression of NSCLC. Finally, our study provides a new theoretical basis for the clinical treatment of NSCLC. Nevertheless, our study still has some shortcomings. First, only two NSCLC cell lines were utilized. Future investigations should include a broader range of cell lines to substantiate our findings. Second, the study lacks experimental verification in animal models. Subsequent studies should further explore the regulatory role of

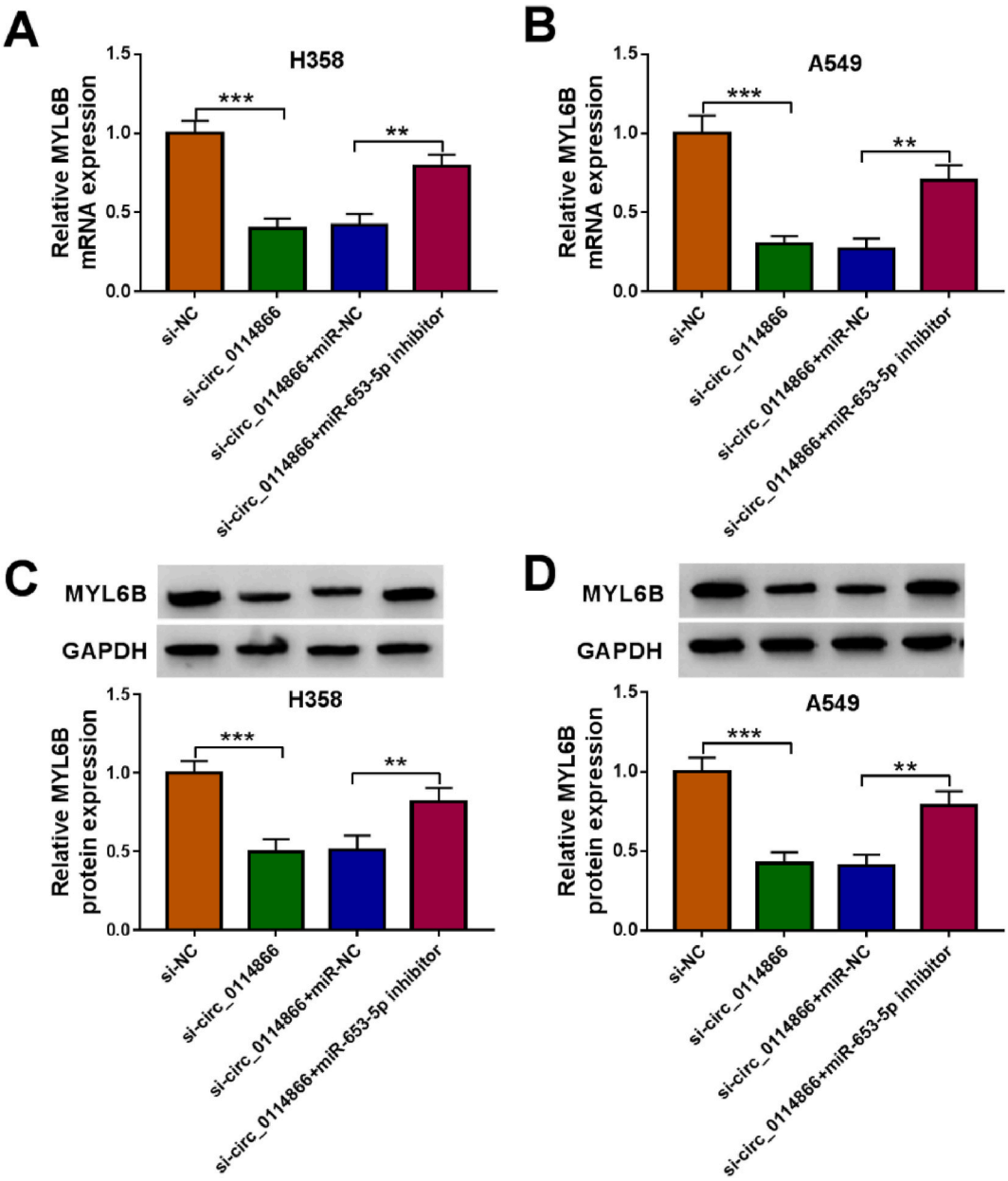

Fig. 8. Circ-0114866 silencing decreased MYL6B expression by sponging miR-653-5p. (A–B) The mRNA level of MYL6B in H358 and A549 cells in each group. (C–D) The protein level of MYL6B in H358 and A549 cells in each group. $^{**}P < 0.01$; $^{***}P < 0.001$. Full Western blot images can be found at Supplementary Materials.

circ_0114866 *in vivo*. Third, our study is not supported by clinical data. Clinical validation of our conclusions is necessary in future research.

5. Conclusion

In summary, we observed the expression of circ_0114866 was increased in NSCLC tissues and cells. Furthermore, circ_0114866 knockdown exhibited a suppressive effect on NSCLC progression and the EMT process. Mechanistic studies revealed that circ_0114866 silencing achieves this regulatory effect by downregulating MYL6B through by sponging miR-653-5p. Our findings imply that circ_0114866 serve as an innovative biomarker for NSCLC.

Ethics statement

The animal study was approved by the Cangzhou Central Hospital Ethics Committee (2020-048-01 (Z)).

CRediT authorship contribution statement

Jinpeng Sun: Writing – review & editing, Writing – original draft, Supervision, Resources, Conceptualization. **Zhenshan Zhang:** Methodology, Investigation, Formal analysis, Data curation. **Binghui Xia:** Writing – original draft, Visualization, Validation, Methodology, Investigation, Data curation. **Tianyu Yao:** Writing – original draft, Investigation, Formal analysis. **Fengyue Ge:** Writing – original draft, Visualization, Methodology. **Fengmei Yan:** Writing – review & editing, Visualization, Validation, Software.

Declaration of competing interest

The authors declare that they have no known competing financial interests or personal relationships that could have appeared to influence the work reported in this paper.

Appendix A. Supplementary data

Supplementary data to this article can be found online at https://doi.org/10.1016/j.heliyon.2024.e37062.

References

[1] Q. Huang, P. Diao, C.L. Li, Q. Peng, T. Xie, Y. Tan, J.Y. Lang, Preoperative platelet-lymphocyte ratio is a superior prognostic biomarker to other systemic inflammatory response markers in non-small cell lung cancer, Medicine (Baltim.) 99 (4) (2020) e18607.
[2] D.A. Huh, M.S. Kang, J. Lee, J.Y. Choi, K.W. Moon, Y.J. Lee, Occupational and environmental asbestos exposure and the risk of lung cancer in Korea: a case-control study in South Chungcheong Province of Korea, PLoS One 16 (4) (2021) e0249790.
[3] X. Chen, X. Cao, W. Xiao, B. Li, Q. Xue, PRDX5 as a novel binding partner in Nrf2-mediated NSCLC progression under oxidative stress, Aging (Albany NY) 12 (1) (2020) 122–137.
[4] W. das Neves, C.R.R. Alves, A.P. de Souza Borges, G. de Castro Jr., Serum creatinine as a potential biomarker of skeletal muscle atrophy in non-small cell lung cancer patients, Front. Physiol. 12 (2021) 625417.
[5] L. Hu, J. Tang, X. Huang, T. Zhang, X. Feng, Hypoxia exposure upregulates MALAT-1 and regulates the transcriptional activity of PTB-associated splicing factor in A549 lung adenocarcinoma cells, Oncol. Lett. 16 (1) (2018) 294–300.
[6] J. Tan, X. Sun, J. Zhang, H. Li, J. Kuang, L. Xu, X. Gao, C. Zhou, Exploratory evaluation of EGFR-targeted anti-tumor drugs for lung cancer based on lung-on-a-chip, Biosensors 12 (8) (2022).
[7] L. Qi, Y. Pan, M. Tang, X. Chen, Circulating cell-free circRNA panel predicted tumorigenesis and development of colorectal cancer, J. Clin. Lab. Anal. 36 (5) (2022) e24431.
[8] H.L. Sanger, G. Klotz, D. Riesner, H.J. Gross, A.K. Kleinschmidt, Viroids are single-stranded covalently closed circular RNA molecules existing as highly base-paired rod-like structures, Proc. Natl. Acad. Sci. U.S.A. 73 (11) (1976) 3852–3856.
[9] Z.H. Deng, G.S. Yu, K.L. Deng, Z.H. Feng, Q. Huang, B. Pan, J.Z. Deng, Hsa_circ_0088233 alleviates proliferation, migration, and invasion of prostate cancer by targeting hsa-miR-185-3p, Front. Cell Dev. Biol. 8 (2020) 528155.
[10] H. Zhou, X. He, Y. He, C. Ou, P. Cao, Exosomal circRNAs: emerging players in tumor metastasis, Front. Cell Dev. Biol. 9 (2021) 786224.
[11] A. Beilerli, I. Gareev, O. Beylerli, G. Yang, V. Pavlov, G. Aliev, A. Ahmad, Circular RNAs as biomarkers and therapeutic targets in cancer, Semin. Cancer Biol. 83 (2022) 242–252.
[12] Q. Yi, J. Feng, Y. Liao, W. Sun, Circular RNAs in chemotherapy resistance of lung cancer and their potential therapeutic application, IUBMB Life 75 (3) (2023) 225–237.
[13] S. Zheng, C. Wang, H. Yan, Y. Du, Blocking hsa_circ_0074027 suppressed non-small cell lung cancer chemoresistance via the miR-379-5p/IGF1 axis, Bioengineered 12 (1) (2021) 8347–8357.
[14] W. Han, L. Wang, L. Zhang, Y. Wang, Y. Li, Circular RNA circ-RAD23B promotes cell growth and invasion by miR-593-3p/CCND2 and miR-653-5p/TIAM1 pathways in non-small cell lung cancer, Biochem. Biophys. Res. Commun. 510 (3) (2019) 462–466.
[15] D.P. Bartel, MicroRNAs: genomics, biogenesis, mechanism, and function, Cell 116 (2) (2004) 281–297.
[16] G.A. Calin, C.M. Croce, MicroRNA signatures in human cancers, Nat. Rev. Cancer 6 (11) (2006) 857–866.
[17] Y.S. Lee, A. Dutta, MicroRNAs in cancer, Annu. Rev. Pathol. 4 (2009) 199–227.
[18] M. Zhang, H. Wang, X. Zhang, F. Liu, miR-653-5p suppresses the growth and migration of breast cancer cells by targeting MAPK6, Mol. Med. Rep. 23 (3) (2021).
[19] X. Qi, D. Chen, W. Yu, L. Wang, L. Liu, X. Tao, Long non-coding RNA PRNCR1 promotes ovarian cancer cell proliferation, migration and invasion by targeting the miR-653-5p/ELF2 axis, Mol. Cell. Biochem. 477 (5) (2022) 1463–1475.
[20] H. Wu, J. Xu, G. Gong, Y. Zhang, S. Wu, CircARL8B contributes to the development of breast cancer via regulating miR-653-5p/HMGA2 Axis, Biochem. Genet. 59 (6) (2021) 1648–1665.
[21] Y. Liu, J. Hsin, H. Kim, P.R. Selvin, K. Schulten, Extension of a three-helix bundle domain of myosin VI and key role of calmodulins, Biophys. J. 100 (12) (2011) 2964–2973.
[22] Z. Maliga, M. Junqueira, Y. Toyoda, A. Ettinger, F. Mora-Bermúdez, R.W. Klemm, A. Vasilj, E. Guhr, I. Ibarlucea-Benitez, I. Poser, et al., A genomic toolkit to investigate kinesin and myosin motor function in cells, Nat. Cell Biol. 15 (3) (2013) 325–334.
[23] Z. Chen, W. Huang, T. Dahme, W. Rottbauer, M.J. Ackerman, X. Xu, Depletion of zebrafish essential and regulatory myosin light chains reduces cardiac function through distinct mechanisms, Cardiovasc. Res. 79 (1) (2008) 97–108.
[24] K.A. Newell-Litwa, R. Horwitz, M.L. Lamers, Non-muscle myosin II in disease: mechanisms and therapeutic opportunities, Dis Model Mech 8 (12) (2015) 1495–1515.
[25] M.A. Hartman, D. Finan, S. Sivaramakrishnan, J.A. Spudich, Principles of unconventional myosin function and targeting, Annu. Rev. Cell Dev. Biol. 27 (2011) 133–155.
[26] X. Xie, X. Wang, W. Liao, R. Fei, N. Wu, X. Cong, Q. Chen, L. Wei, Y. Wang, H. Chen, MYL6B, a myosin light chain, promotes MDM2-mediated p53 degradation and drives HCC development, J. Exp. Clin. Cancer Res. 37 (1) (2018) 28.

[27] D. Pan, M. Zheng, J. Liu, Z. Sun, X. Shi, Garlic extract participates in the proliferation and apoptosis of nonsmall cell lung cancer cells via endoplasmic reticulum stress pathway, Evid Based Complement Alternat Med 2023 (2023) 4025734.
[28] X. Yang, F. Shao, S. Shi, X. Feng, W. Wang, Y. Wang, W. Guo, J. Wang, S. Gao, Y. Gao, et al., Prognostic impact of metabolism reprogramming markers acetyl-CoA synthetase 2 phosphorylation and ketohexokinase-A expression in non-small-cell lung carcinoma, Front. Oncol. 9 (2019) 1123.
[29] X. Wang, S. Liu, B. Xu, Y. Liu, P. Kong, C. Li, B. Li, circ-SIRT1 promotes colorectal cancer proliferation and EMT by recruiting and binding to eIF4A3, Anal. Cell Pathol. 2021 (2021) 5739769.
[30] H. Xie, J. Yao, Y. Wang, B. Ni, Exosome-transmitted circVMP1 facilitates the progression and cisplatin resistance of non-small cell lung cancer by targeting miR-524-5p-METTL3/SOX2 axis, Drug Deliv. 29 (1) (2022) 1257–1271.
[31] Z.Y. Zhang, X.H. Gao, M.Y. Ma, C.L. Zhao, Y.L. Zhang, S.S. Guo, CircRNA_101237 promotes NSCLC progression via the miRNA-490-3p/MAPK1 axis, Sci. Rep. 10 (1) (2020) 9024.
[32] R. Chen, F. Liang, J. Yan, Y. Wang, CircCDK17 knockdown inhibits tumor progression and cell glycolysis by downregulaing YWHAZ expression through sponging miR-1294 in cervical cancer, J. Ovarian Res. 15 (1) (2022) 24.
[33] N. Wu, H. Song, Y. Ren, S. Tao, S. Li, DGUOK-AS1 promotes cell proliferation in cervical cancer via acting as a ceRNA of miR-653-5p, Cell Biochem. Funct. 38 (7) (2020) 870–879.
[34] Z. Xing, S. Li, Z. Liu, C. Zhang, Z. Bai, CircSERPINA3 regulates SERPINA3-mediated apoptosis, autophagy and aerobic glycolysis of prostate cancer cells by competitively binding to MiR-653-5p and recruiting BUD13, J. Transl. Med. 19 (1) (2021) 492.
[35] Y. Jin, X. Che, X. Qu, X. Li, W. Lu, J. Wu, Y. Wang, K. Hou, C. Li, X. Zhang, et al., Corrigendum: CircHIPK3 promotes metastasis of gastric cancer via miR-653-5p/miR-338-3p-NRP1 Axis under a long-term hypoxic microenvironment, Front. Oncol. 11 (2021) 783320.
[36] M. Chen, J. Zhang, J. Zeng, Y. Yu, C. Gu, Circular circRANGAP1 Contributes to Non-small Cell Lung Cancer Progression by Increasing COL11A1 Expression through Sponging miR-653-5p, Biochem Genet, 2023.
[37] M. Kovács, J. Tóth, C. Hetényi, A. Málnási-Csizmadia, J.R. Sellers, Mechanism of blebbistatin inhibition of myosin II, J. Biol. Chem. 279 (34) (2004) 35557–35563.